Inorganic Chemistry
Article

Inorg. Chem. **2010**, *49*, 5285–5292 **5285**
DOI: 10.1021/ic100359v

Cation Size and Anion Anisotropy in Structural Chemistry of Metal Borohydrides. The Peculiar Pressure Evolution of $RbBH_4$

Yaroslav Filinchuk,*,† Alexandr V. Talyzin,‡ Hans Hagemann,§ Vladimir Dmitriev,† Dmitry Chernyshov,† and Bertil Sundqvist‡

†*Swiss-Norwegian Beamlines at ESRF, BP-220, 38043 Grenoble, France,* ‡*Department of Physics, Umeå University, 90187 Umeå, Sweden, and* §*Département de Chimie Physique, University of Geneva, 1211 Geneva, Switzerland*

Received February 23, 2010

The pressure evolution of $RbBH_4$ has been characterized by synchrotron powder X-ray diffraction and Raman spectroscopy up to 23 GPa. Diffraction experiments at ambient temperature reveal three phase transitions, at 3.0, 10.4, and 18 GPa (at 2.6, 7.8, and ∼20 GPa from Raman data), at which the space group symmetry changes in the order *Fm*-3*m*(*Z*=4) → *P*4/*nmm*(2) → *C*222(2) → *I*-42*m*(4). Crystal structures and equations of state are reported for all four phases. The three high-pressure structure types are new in the crystal chemistry of borohydrides. $RbBH_4$ polymorphs reveal high coordination numbers (CNs) for cation and anion sites, increasing with pressure from 6 to 8, via an intermediate 4 + 4 coordination. Different arrangements of the tetrahedral BH_4 group in the Rb environment define the crystal symmetries of the $RbBH_4$ polymorphs. The structural evolution in the MBH_4 series is determined by the cation's size, as it differs drastically for M = Li (CNs = 4, 6), Na (CN = 6), and Rb. The only structure common to the whole MBH_4 family is the cubic one. Its bulk modulus linearly decreases as the ionic radius of M increases, indicating that the compressibility of the material is mainly determined by the repulsive $BH_4\cdots BH_4$ interactions.

Introduction

Owing to their high gravimetric hydrogen density, metal borohydrides are seen as promising materials for energy storage. Some borohydrides desorb a large quantity of hydrogen (up to 20.8%), although the decomposition temperatures are usually high.[1] The search for better hydrogen storage materials, with denser structures and lower binding energies, has been hampered by a lack of basic knowledge about their structural properties. However, the past few years have seen a remarkably rapid evolution of this field, and a large number of experimental and theoretical studies have recently been carried out, as summarized in several very recent reviews on crystal structures,[2] physical properties,[3] and phase relations[4] in borohydrides at different $P-T$ conditions. These experimental investigations have already revealed a surprising multitude of novel and unexpected structural phases, most of which were not predicted by calculations. The structural phases and phase diagrams of the most important light hydrides $LiBH_4$,[5−8] $NaBH_4$,[9−13] and the related NH_3BH_3[14] have already been experimentally identified and mapped. For heavier borohydrides, KBH_4 and $RbBH_4$, the high-pressure studies have just begun.[15−17]

In the present paper we report a synchrotron X-ray diffraction study of the structural evolution of $RbBH_4$ under pressure at room temperature. In the range up to 23 GPa, four different structural phases are found, with transition pressures of about 3.0, 10.4, and 18 GPa. The phase transitions have also been observed by *in situ* Raman scattering experiments under pressure. The space group symmetry

*To whom correspondence should be addressed. Tel: +33 47 688 2775. Fax: +33 47 688 2694. E-mail: Yaroslav.Filinchuk@esrf.fr.

(1) Soloveichik, G. *Mater. Matters* (*Aldrich*) **2007**, *2*, 11–14.
(2) Filinchuk, Y.; Chernyshov, D.; Dmitriev, V. *Z. Kristallogr.* **2008**, *223*, 649–659.
(3) Sundqvist, B.; Andersson, O. *Int. J. Thermophys.* **2009**, *30*, 1118–1129.
(4) Sundqvist, B. *Solid State Phenom.* **2009**, *150*, 175–195.
(5) Talyzin, A. V.; Andersson, O.; Sundqvist, B.; Kurnosov, A; Dubrovinsky, L. *J. Solid State Chem.* **2007**, *180*, 510–517.
(6) Filinchuk, Y.; Chernyshov, D.; Nevidomskyy, A.; Dmitriev, V. *Angew. Chem., Int. Ed.* **2008**, *47*, 529–532.
(7) Dmitriev, V.; Filinchuk, Y.; Chernyshov, D.; Talyzin, A. V.; Dzwilewski, A.; Andersson, O.; Sundqvist, B.; Kurnosov, A. *Phys. Rev. B* **2008**, *77*, 174112.
(8) Filinchuk, Y.; Chernyshov, D.; Černý, R. *J. Phys. Chem. C* **2008**, *112*, 10579–10584.
(9) Kumar, R. S.; Cornelius, A. L. *Appl. Phys. Lett.* **2005**, *87*, 261916.
(10) Araújo, C. M.; Ahuja, R.; Talyzin, A. V.; Sundqvist, B. *Phys. Rev. B* **2005**, *72*, 054125.
(11) Sundqvist, B.; Andersson, O. *Phys. Rev. B* **2006**, *73*, 092102.
(12) Filinchuk, Y.; Talyzin, A. V.; Chernyshov, D.; Dmitriev, V. *Phys. Rev. B* **2007**, *76*, 092104.
(13) Babanova, O.; Soloninin, A.; Stepanov, A.; Skripov, A.; Filinchuk, Y. *J. Phys. Chem. C* **2010**, *114*, 3712.
(14) Filinchuk, Y.; Nevidomskyy, A. H.; Chernyshov, D.; Dmitriev, V. *Phys. Rev. B* **2009**, *79*, 214111.
(15) Kumar, R. S.; Kim, E.; Cornelius, A. L. *J. Phys. Chem. C* **2008**, *112*, 8452–8457.
(16) Kumar, R. S.; Cornelius, A. L. *J. Alloys Compd.* **2009**, *476*, 5–8.
(17) Sundqvist, B.; Andersson, O.; Talyzin, A. V. *J. Phys.: Condens. Matter* **2007**, *19*, 425201.

Published on Web 05/13/2010

Table 1. Rietveld-Refined Structural Parameters for the $RbBH_4$ Polymorphs Obtained in the High-Pressure Diffraction Experiments at Room Temperature[a]

structure	atom	Wyckoff site	x	y	z	B, Å^2
Fm-3*m*, $Z = 4$	Rb	4*a*	0	0	0	3.80(3)
$a = 6.96330(7)$ Å at 0.5 GPa	B	4*b*	1/2	1/2	1/2	7.3(3)
	H	32*f* (occ. 1/2)	0.410	*x*	*x*	9.3(3)
*P*4/*nmm* (choice 2), $Z = 2$	Rb	2*c*	1/4	1/4	0.34634(2)	2.69(3)
$a = 5.61216(13)$	B	2*a*	1/4	3/4	0	6.0(3)
$b = 4.08873(14)$ Å at 5.5 GPa	H	8*i*	0.427	3/4	0.174	8.0(3)
*C*222, $Z = 2$	Rb	2*a*	0	0	0	3.0(2)
$a = 5.3679(6)$, $b = 5.1343(14)$	B	2*c*	1/2	0	1/2	4.0(5)
$c = 3.9098(3)$ Å at 16.1 GPa	H	8*l*	0.380	0.121	0.327	6.0(5)
I-42*m*, Z = 4	Rb	4*e*	0	0	0.2329(4)	2.11(4)
$a = 5.0057(7)$	B	4*c*	0	1/2	0	2.4(4)
$c = 7.8161(13)$ Å at 23.5 GPa	H	16*j*	0.125	0.375	0.080	4.4(4)

[a] Positions of hydrogen atoms were not refined.

changes in the order *Fm*-3*m* → *P*4/*nmm* → *C*222 → *I*-42*m*; none of the three high-pressure structure types have been observed or predicted earlier for the borohydrides. We propose that the structural properties of borohydrides are determined by the size of the alkali metal ions, and the different arrangements of the tetrahedral BH_4 group in the metal atom environment define the crystal symmetries of the high-pressure polymorphs. In addition to structural data, we also present experimental results for the bulk compressibility and for the individual Grüneisen parameters of the Raman-active phonon modes.

Experimental Section

Synthesis. $RbBH_4$ was prepared as previously reported[18] by the reaction of RbOH with $NaBH_4$ in cold (ca. −10 °C) methanol. RbOH is first dissolved in CH_3OH and the solution is cooled. A second flask containing CH_3OH is precooled using a salt−ice mixture; then 1.05 equiv of $NaBH_4$ is dissolved in the cold CH_3OH. The two cold solutions are mixed, and the precipitate is filtered off and dried under vacuum.

The pure deuterides can also be prepared using this method, using RbOD, $NaBD_4$, and CH_3OD. The use of RbOH and CH_3OH in conjunction with $NaBD_4$ leads to the formation of some $RbBD_3H$ impurities. Thus, a mixed $RbBD_4/RbBD_3H$ sample was obtained by the reaction of RbOH with $NaBD_4$ (CIL, ca. 98% isotopically pure) in cold (ca. −5 °C) methanol. Comparative Raman spectra of the pure $RbBD_4$ and the isotopically mixed sample are shown in the Supporting Information (Figures S1 and S2).

High-Pressure Diffraction Experiments. Diffraction patterns were collected at the Swiss−Norwegian Beamlines of the ESRF using a MAR345 image plate detector and a monochromatic beam with the wavelength of 0.72287 or 0.70000 Å. The wavelengths, sample-to-detector distance (200 or 250 mm), and parameters of the detector were calibrated using NIST standard LaB_6. Two-dimensional diffraction images were integrated using Fit2D software.[19] Finely ground samples were loaded into diamond anvil cells (DACs) with flat culets of 600 μm diameter. The samples were loaded into a hole of 200−250 μm in diameter drilled in stainless steel gaskets preindented to 60−80 μm thickness; the beam was slit-collimated to 100 × 100 μm^2. Ruby provided a pressure calibration with a precision of 0.1 GPa. No pressure-transmitting medium was used. In order to control pressure gradients across the sample, two ruby chips were loaded into the DAC: one in the hole center and the other near the hole border. Estimated ΔP across the beam was less than 1.5 GPa at the higher end of the pressure range, which represents the upper end of the accuracy of pressure measurements. Pressures mentioned hereafter relate to the cell center. Diffraction measurements were performed up to a maximum pressure of 23 GPa.

Raman Spectroscopy. A Renishaw Raman 1000 spectrometer with 633 and 514 nm excitation lasers and a resolution of 2 cm^{-1} was used in these experiments. Raman spectra were recorded *in situ* through the diamond anvils using a long-focus 50× objective in 0.5−1 GPa pressure steps. Spectra for the starting material and for the sample loaded into the DAC were identical. Usually, the total time spent at each pressure step, allowing for the pressure stabilization and the data collection, was about 1−2 h.

Results and Discussion

A. Crystal Structures of $RbBH_4$ Polymorphs. Atomic and cell parameters for the four $RbBH_4$ polymorphs are listed in Table 1. The Rietveld refinement profiles are shown in the Supporting Information (Figure S3).

***Fm*-3*m* Phase.** The crystal structure of the ambient-pressure phase is cubic, space group *Fm*-3*m* with 4 formula units in the unit cell. It has a NaCl-type arrangement of Rb cations and BH_4 anions, where the latter are orientationally disordered over the two positions around the inversion center. The disordered centrosymmetric structure for the cubic $RbBH_4$ was assumed by the analogy to the well-established structure of $NaBH_4$.[20] The position of the H atom was fixed, and two atomic displacement parameters (for Rb and BH_4) were refined. Similar to the $NaBH_4$ phases,[12,21] the cubic $RbBH_4$ in a DAC reveals a pronounced preferred orientation (PO). The PO along the [100] direction was modeled by one parameter (March's function), which appears to be nearly pressure-independent, at a value of ∼0.8. Some anisotropic peak broadening developing at higher pressures was modeled as a uniaxial microstrain along [111] using one refined parameter. In total, 16 reflections were fitted with three intensity-dependent parameters. The refinement with the help of Fullprof software[22] converged at $R_B = 4.9\%$, $R_F = 3.6\%$, $R_p = 0.41\%$, $R_{wp} = 0.72\%$ (not corrected for background), and $R_p = 8.7\%$, $R_{wp} = 6.4\%$ (conventional).

(18) Hagemann, H.; Gomes, S.; Renaudin, G.; Yvon, K. *J. Alloys Compd.* **2004**, *363*, 129–132.
(19) Hammersley, A. P.; Svensson, S. O.; Hanfland, M.; Fitch, A. N.; Häusermann, D. *High Pressure Res.* **1996**, *14*, 235–248.
(20) Filinchuk, Y.; Hagemann, H. *Eur. J. Inorg. Chem.* **2008**, 3127–3133.
(21) Chernyshov, D.; Bosak, A.; Dmitriev, V.; Filinchuk, Y.; Hagemann, H. *Phys. Rev. B* **2008**, *78*, 172104.
(22) Rodrigues-Carvajal, J. *Phys. B* (*Amsterdam, Neth.*) **1993**, *192*, 55–69.

***P*4/*nmm* Phase.** A transition from the cubic to a new high-pressure phase starts at 3 GPa and completes at 3.4 GPa. First 16 diffraction peaks were indexed by Dicvol[23] in a primitive tetragonal cell with a volume slightly over one-half that of the cubic structure. Analysis of systematic absences using the program ChekCell[24] suggested two possible space groups: *P*4/*n* and *P*4/*nmm*. A database search suggested that this phase may be an antitype (positions of cation and anion are interchanged) of NH_4Br.[25] A good fit to the data confirmed this suggestion. Thus, the position of the hydrogen atom was assumed by the similarity to the NH_4Br structure. A small PO along [001] was modeled by one refined parameter, which converged to 0.9635(14) at 5.5 GPa; its value is systematically smaller than 1 on compression and larger than 1 on decompression. In total, 38 reflections were fitted with only four intensity-dependent parameters, including one coordinate parameter. The refinement converged at $R_B = 4.0\%$, $R_F = 3.9\%$, $R_p = 0.36\%$, $R_{wp} = 0.51\%$ (not corrected for background), and $R_p = 7.8\%$, $R_{wp} = 5.5\%$ (conventional).

***C*222 Phase.** Above 10.4 GPa the *P*4/*nmm* phase starts to transform into a new phase, and this transformation completes at ~12.2 GPa. Thirteen peak positions were extracted from a data set collected at 16.1 GPa and indexed by Dicvol[23] in a monoclinic cell. Although its unit cell volume allowed only one $RbBH_4$ unit per unit cell, the structure could not be solved in any of the possible monoclinic space groups. Therefore, similar to the case of the high-pressure structure of $LiBH_4$,[6] we attempted a structure solution in the space group *P*1. The structure has been solved in *P*1 by a global optimization in direct space using the program FOX.[26] Starting with this model, a *C*-centered orthorhombic structure with 2 times larger volume was uncovered by Platon software.[27] Only after taking into account a pronounced PO along [010] was the structure successfully refined in the space group *Cmmm*. Rb and B atoms were reliably located in the special positions. The resulting atomic arrangement represents an orthorhombically distorted CsCl-type structure, and to the best of our knowledge it has no analogues, at least none that may suggest possible positions of hydrogen atoms. Our analysis shows that a fully ordered BH_4 group can be accommodated in two subgroups of *Cmmm*: in *Cmm*2, where nearly linear B−H···Rb fragments lead to unlikely short H···Rb contacts; and in *C*222, where Rb···H and H···H distances can be kept sufficiently long. Thus, we finally assumed the ordered *C*222 model for this phase. In the final refinement, a strong PO along [010] was modeled by one refined parameter, which converged to 1.542(10). In total, 33 reflections were fitted with five intensity-dependent parameters, including three anisotropic displacement factors for the Rb atom, yielding a reasonable displacement ellipsoid ($B_{11} = 2.42(12)$, $B_{22} = 4.7(5)$, $B_{33} = 1.76(11)$ Å^2). The refinement converged at $R_B = 5.8\%$, $R_F = 5.2\%$, $R_p = 0.67\%$, $R_{wp} = 1.05\%$ (not corrected for background), and $R_p = 13.7\%$, $R_{wp} = 10.9\%$ (conventional).

***I*-42*m* Phase.** First traces of yet another phase appear at ~17 GPa. The transition is not fully completed even at the highest pressure achieved in our experiment. However, the six most pronounced peaks were unambiguously indexed in a body-centered tetragonal cell, suggesting four $RbBH_4$ units per unit cell. Metrically, this tetragonal structure is closely related to the *C*222 one, with the *a* and *b* parameters of the latter becoming equal and the *c* parameter doubled. Similar to the *C*222 phase, the new structure also roughly resembles the CsCl-type, but a closer analysis was required to reveal a more detailed picture. The superstructure peaks 101 and 103 can be clearly observed, and they cannot be modeled in the space groups containing 4 or 4_2 axes: these peaks indicate a corrugated distortion of the CsCl-type, which involves a displacement of the heavy atom (Rb) along the *c* axis. Such displacement can be accommodated in the space group *I*-4 and its supergroups. A good fit to the experimental data was accomplished in the space groups *I*-4*m*2 and *I*-42*m*, where the latter allows longer Rb···H distances for the ordered BH_4 group. To our knowledge, this structure, like the *C*222 one, represents a new structure type derived from the CsCl type. A *I*-42*m* structural model well approximating the experimental data was first created in FOX[26] and then refined by the Rietveld method. A PO along [100], very similar to the one in the *C*222 phase, was modeled by one refined parameter, which converged to 1.576(14). In total, 36 reflections were fitted with four intensity-dependent parameters, including one coordinate parameter. For the two-phase samples containing *C*222 and *I*-42*m* phases the atomic displacement factors for the identical atom types were constrained to be the same, thus reducing the number of parameters intrinsic to the *I*-42*m* phase to two. For the sample containing ~50% of the *I*-42*m* phase (23.5 GPa), the refinement converged at $R_B = 8.3\%$, $R_F = 6.3\%$, $R_p = 0.57\%$, $R_{wp} = 0.80\%$ (not corrected for background), and $R_p = 12.0\%$, $R_{wp} = 9.9\%$ (conventional).

B. Pressure Evolution of the Unit Cell Dimensions. We find three phase transitions at 3.0, 10.4, and 18 GPa, all of them of first order. Two decompression experiments showed that the first two transitions are reversible. The decompression experiment was not made for the highest pressure *I*-42*m* phase. However, since the last transition is not reconstructive, we expect it also to be reversible. The ambient-pressure *Fm*-3*m* polymorph transforms into the new *P*4/*nmm* phase with a remarkable volume collapse of 8.8% and with a small hysteresis of ~0.4 GPa. Interestingly, in a narrow pressure range, starting just below the cubic-to-tetragonal transition, we observed additional diffraction lines which do not originate from the *Fm*-3*m* and *P*4/*nmm* phases. These peaks show a maximum intensity at ~2.75 GPa (*d*-spacings: 4.015, 3.877, 2.327, and 1.996 Å). However, they always coexist with peaks of the *Fm*-3*m* or the *P*4/*nmm* phases or from both phases. Taking into account that the space group symmetry change *Fm*-3*m*(number of formula units per primitive cell $Z_P = 1$) → *P*4/*nmm*($Z_P = 2$) breaks the group−subgroup relationship, this observation might be explained by the onset of an intermediate (possibly metastable) phase, which emerges during this reconstructive transition accompanied by the big volume drop.

The experimental unit cell volumes were fitted with the Murnaghan equation of state (EOS), yielding molecular volumes at zero pressure and the bulk moduli

(23) Boultif, A.; Louer, D. *J. Appl. Crystallogr.* **2004**, *37*, 724–731.
(24) Laugier, J.; Bochu, B. *LMGP suite for Windows*, Laboratoire des Materiaux et du Génie Physique de l'Ecole, Supérieure de Physique de Grenoble, http://www.inpg.fr/LMGP.
(25) Levy, H. A.; Peterson, S. W. *J. Am. Chem. Soc.* **1953**, *75*, 1536–1542.
(26) Favre-Nicolin, V.; Černý, R *J. Appl. Crystallogr.* **2002**, *35*, 734–743.
(27) Spek, A. L. *PLATON*; University of Utrecht: The Netherlands, **2006**.

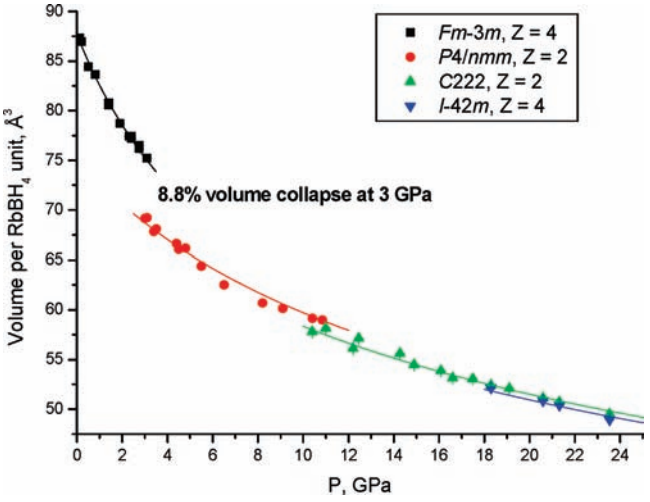

Figure 1. Pressure variation of the volume of the $RbBH_4$ formula unit at ambient temperature. The symbols represent experimental data for four different phases obtained in three independent experiments; the lines are the best fits to the Murnaghan equation of state.

(their pressure derivatives B'_0 were fixed at 3.5). Figure 1 includes all reliable data points measured in three independent experiments; only the data obtained during the compression were used for the calculation of EOS. The two transitions at higher pressures manifest small volume contractions: ~2.2% for the *P*4/*nmm* → *C*222 transition at 10.4 GPa and ~1.1% for the *C*222 → *I*-42*m* transition. The latter transformation starts at ~18 GPa and is not fully accomplished until at the highest pressure achieved in our experiment: at a pressure of 23.5 GPa, about 48% of the *C*222 phase remained. Heating the sample in the DAC at 20 GPa to 100 °C and cooling to room temperature still did not produce pure *I*-42*m* phase.

Compressibilities of the high-pressure phases of $RbBH_4$ are anisotropic: the *c*/*a* ratio for the *P*4/*nmm* phase increases linearly with pressure, from 0.7267 at 3.0 GPa to 0.7337 at 10.4 GPa. The compressibility of the *C*222 phase is even more anisotropic: along the *b* axis the structure is nearly twice more compressible than along *a* and *c*. However, the variation of the axial ratios from the *P*4/*nmm* to the *C*222 phase is practically continuous (see Figure S4 in the Supporting Information). Some discontinuity appears on the *C*222 → *I*-42*m* transition: the *a* parameter of the *I*-42*m* structure is slightly smaller than the average of the *a* and *b* of the pseudotetragonal *C*222, while the doubled *c* axis is slightly larger than 2*c* of the *C*222 phase. Thus, the axial ratio for the $RbBH_4$ phases increases with pressure from 0.707 to 0.780 (Figure S4), moving away from the $1/\sqrt{2} = 0.707$ value for the ideal NaCl and CsCl-type structures.

Table 2 lists EOS data for the alkali metal borohydrides from the literature and from the present work. Note that the true bulk modulus determined from an inelastic scattering study of the acoustic phonon dispersions is lower than the ones from high-pressure experiments in DACs.[21] The packing efficiencies of various structures are closely related with their compressibilities: for each system, a larger volume drop at a transition results in a proportional decrease in compressibility (the inverse of the bulk modulus). Among all the borohydrides, $RbBH_4$ has the largest number of pressure-driven phase transitions. The only structure common to the whole MBH_4 family is the cubic one (note that the *Pnma*

Table 2. Experimental Equation of State Parameters for Alkali Metal Borohydrides at Room Temperature

compound	phase	molar V_0 [Å^3]	B_0 [GPa]	B'_0	method	ref
$LiBH_4$	*Pnma*	54.43(8)	14.4(5)	3.5 (fixed)	XRD	6
	*Ama*2	49.49(13)	23.23(9)	3.51(15)	XRD	6
	Fm-3*m*	47.3(9)	26(3)	3.5 (fixed)	XRD	6
$NaBH_4$	*Fm*-3*m*	58.3(2)	19(1)	3.1(3)	XRD	21
			15.8		IXS	21
			19.9(7)	3.5 (fixed)	XRD	9
$NaBH_4$	*Pnma*		31(1)	3.9 (fixed)	XRD	9
KBH_4	*Fm*-3*m*		16.8(4)	4 (fixed)	XRD	15
$RbBH_4$	*Fm*-3*m*	87.7(2)	14.9(4)	3.5 (fixed)	XRD	this work
			14.5(2)	4 (fixed)	XRD	16
	*P*4/*nmm*	75.3(7)	28(2)	3.5 (fixed)	XRD	this work
	*C*222	73.2(18)	29(4)	3.5 (fixed)	XRD	this work
	I-42*m*	72	30	3.5 (fixed)	XRD	this work

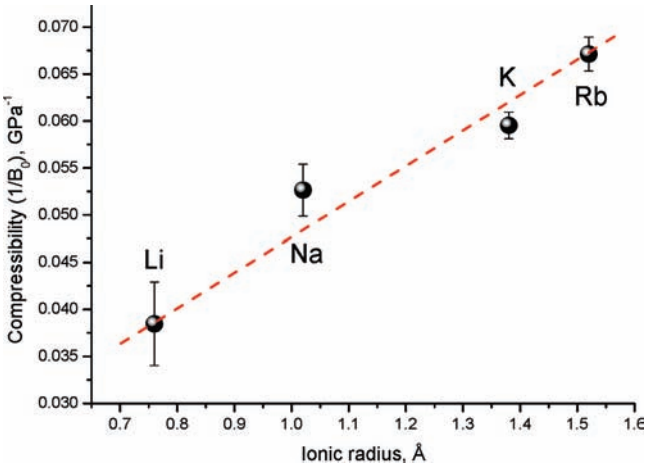

Figure 2. Dependence of the compressibility (inverse of the experimental bulk moduli) of the cubic MBH_4 phases versus the ionic radius of M (the radii are taken from ref 28 for CN = 6). The experimental uncertainties are depicted as error bars.

phases of $LiBH_4$ and $NaBH_4$ have completely different structures[12]). The bulk moduli for the cubic phases decrease from the light to heavy borohydrides, ranging from 26(3) GPa for $LiBH_4$ to 14.9(4) GPa for $RbBH_4$. Our analysis reveals a practically linear dependence of the compressibility (inverse of the bulk modulus) of the cubic MBH_4 on the ionic radius[28] of M (see Figure 2). As the radius of M increases, the repulsive H···H contacts between the BH_4 groups weaken and become more compressible. Thus the change of the bulk modulus in the series of cubic MBH_4 is largely defined by the compressibility of the anion substructure, dominated by the repulsive H···H interactions.

C. Crystal Chemistry of $RbBH_4$ and Comparison with Other Alkali Metal Borohydrides. The ambient-pressure cubic phase is isostructural to $NaBH_4$, where the BH_4 group is disordered over two positions.[20] Its partial ordering at low temperature was detected at 44 K,[29] without a reconstruction or a change of the atomic coordination numbers (CN).[30] The high-pressure structures are ordered, at least regarding the positions of the Rb and B atoms. Although hydrogen atoms cannot be

(28) Shannon, R. D. *Acta Crystallogr. A* **1976**, *32*, 751–767.
(29) Stephenson, C. C.; Rice, D. W.; Stockmayer, W. H. *J. Chem. Phys.* **1955**, *23*, 1960.
(30) Renaudin, G.; Gomes, S.; Hagemann, H.; Keller, L.; Yvon, K. *J. Alloys Compd.* **2004**, *375*, 98–106.

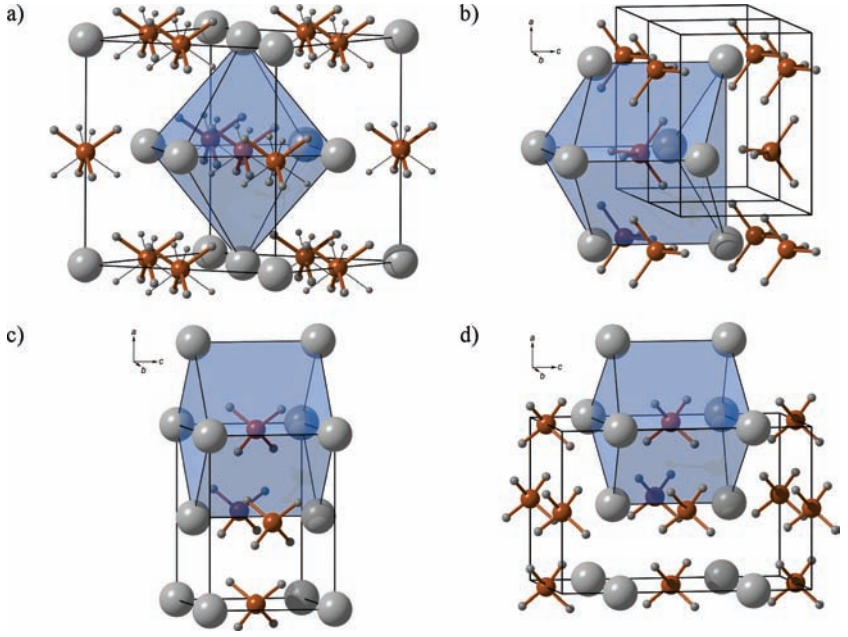

Figure 3. Crystal structures of $RbBH_4$ polymorphs showing the changes of the coordination polyhedra for the BH_4 group under pressure: *Fm*-3*m* (a), *P*4/*nmm* (b), *C*222 (c), and *I*-42*m* (d). Two orientations of the disordered BH_4 group in the cubic phase (a) are shown by bold and thin lines.

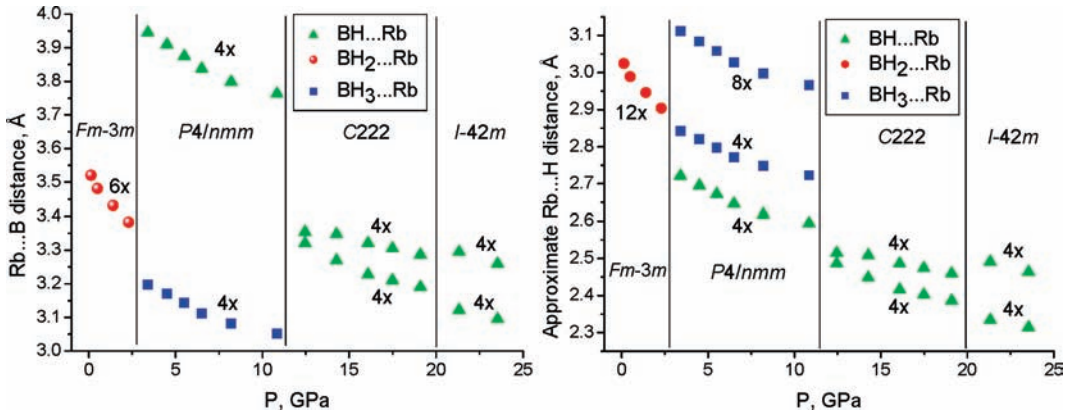

Figure 4. Pressure evolution of Rb···B (left) and Rb···H (right) distances in the four $RbBH_4$ polymorphs. Different symbols distinguish three different types of BH_4···Rb interaction: via a vertex (green triangles), an edge (red circles), and a face (blue squares) of the tetrahedral BH_4 group.

directly detected from synchrotron X-ray diffraction data in the presence of much heavier Rb, they can be located as a part of the rigid tetrahedral BH_4 group. The latter possibility is based on the tetrahedral geometry of the BH_4 group found in light metal borohydrides by accurate single-crystal X-ray diffraction.[8,20,31−34] Despite an earlier controversy, it was concluded[2] that except for a few specific cases the BH_4 group has a nearly ideal tetrahedral geometry. This geometrical constraint, combined with the high point group symmetries of the BH_4 sites, allowed the location of the H atoms in the high-pressure $RbBH_4$ phases.

All four $RbBH_4$ phases have very simple crystal structures, each containing a single Rb, B, and H position (see Table 1). The *P*4/*nmm* phase is an antitype to ammonium and phosphonium bromides and iodides,[25] while the *C*222 and *I*-42*m* phases represent two new structure types, which are the deformation variants of the cubic CsCl-type structure. As expected, the refined atomic displacement factors (Table 1) decrease at higher pressures, thus supporting our structural determinations.

It is interesting that the high-pressure transitions involve changes of the CN for the cation's and anion's sites as well as the changes in the Rb···BH_4 coordination mode. Figure 3 displays the $RbBH_4$ structures and the coordination polyhedra for the BH_4 group. The octahedral coordination in the ambient-pressure phase gradually transforms to a more or less distorted cubic arrangement at higher pressures. The average Rb···B distances correlate with the change of the CN: upon the first transition, CN goes from 6 to 4 + 4 and the average Rb···B distance increases by ~7% and then smoothly decreases at higher pressures. A combination of different BH_4 coordination modes together with the increase in CN leads to an increase in density by 8.8% at the cubic-to-tetragonal phase transition, in spite of the fact that the average Rb···B distance increases. The specific Rb···B and

(31) Marynick, D. S.; Lipscomb, W. N. *Inorg. Chem.* **1972**, *11*, 820–823.
(32) Aldridge, S.; Blake, A. J.; Downs, A. J.; Gould, R. O.; Parsons, S.; Pulham, C. R. *J. Chem. Soc., Dalton Trans.* **1997**, 1007–1012.
(33) Filinchuk, Y. E.; Yvon, K.; Meisner, G. P.; Pinkerton, F. E.; Balogh, M. P. *Inorg. Chem.* **2006**, *45*, 1433–1435.
(34) Filinchuk, Y.; Černý, R.; Hagemann, H. *Chem. Mater.* **2009**, *21*, 925–933.

Rb···H distances show a large spread (Figure 4), related to the occurrence of the three different Rb···BH_4 coordination modes: via a face, an edge, and a vertex of the tetrahedral anion. The BH_4 group acts with respect to the metal atom as a mono-, di-, and trihapto ligand, similar to other borohydrides and their solvates.[2,35] However, this is the first time that all three coordination modes are found in different polymorphic modifications of the same compound.

The CN for Rb atoms can be defined with respect to the nearest BH_4 sites and with respect to the coordinated hydrogen atoms. As can be seen from Figure 4, the first one changes regularly with increasing pressure in the sequence 6, 4 + 4, 8, 8; the second irregularly, −12, 16, 8, 8. The CNs and coordination modes are closely linked to the corresponding Rb···B and Rb···H distances. In the cubic phase, each Rb atom is surrounded by six η^2-BH_4 groups at equal distances (η^2 corresponds to the coordination via a tetrahedral edge). The number of BH_4 neighbors increases to eight in the *P*4/*nmm* phase. Due to the change of the BH_4 coordination mode, the corresponding interatomic distances are segregated into four short Rb···B of 3.05−3.2 Å (12 long Rb···H of 2.7−3.1 Å) distances for the η^3-BH_4 coordination and four long Rb···B of 3.76−3.95 Å (four short Rb···H of 2.6−2.7 Å) distances for the η^1-BH_4 coordination (η^1 and η^3 stand respectively for the coordination via a vertex and a face). The *P*4/*nmm* structure is derived from the cubic by shifting the Rb atom and the BH_4 group along the *c* axis of the resulting tetragonal cell. The *z*-coordinate for the Rb atom is the only refined coordinate in this structure. The value of $z = 1/4$ corresponds to the regular Rb_6 octahedra, centered by the BH_4 anion in the initial cubic structure. However, the *P*4/*nmm* phase is stable at higher *z*, which equals 0.34634(2) at 5.5 GPa and slightly increases with pressure. The situation with $z = 0.5$ would bring the structure to the CsCl type, but this value is not within the observed limits of the structural stability at room temperature. Instead, the *C*222 and *I*-42*m* phases appear with structures closely related to the CsCl type. Thus, the *P*4/*nmm* structure is intermediate between the NaCl and CsCl types, and the transitions occur by the mechanism of atomic displacements.

The ideal CsCl-type structure is not met in $RbBH_4$ owing to the better packing of the anisotropic anions and spherical cations in the distorted structures. The arrangement of the BH_4 group inside the Rb_8 cube, with η^1-BH_4 pointing the B−H bonds toward the midpoint between two Rb atoms, is likely the densest one, as it is practically the same in the higher pressure *C*222 and *I*-42*m* phases (Figure 3). Thus, the observed distortions of the parent CsCl-type structure are the result of an interplay between the ordered BH_4 group and its cubic Rb_8 environment. Different arrangements of the tetrahedral BH_4 group in the Rb environment result in different point group symmetries of the BH_4 anions, namely, −4*m*2 (D_{2d}) in the *P*4/*nmm* structure and 222 (D_2) in the *C*222 and *I*-42*m* structures, and define the crystal symmetries of the high-pressure $RbBH_4$ polymorphs. On the contrary, alkali metal halides, containing spherical cations and anions, show the high-symmetry cubic structures at various *P*−*T* conditions.[36]

It is striking that the symmetry and structures of all high-pressure $RbBH_4$ phases differ from both those predicted theoretically (*P*-42$_1$*c* or *P*4$_2$/*nmc*)[37] and those (*Pnma* and *P*2/*c*, both with undefined structure) suggested on the basis of diffraction data.[16] Our study shows that the structural chemistry of $RbBH_4$ under pressure is not identical to that of $NaBH_4$, as originally proposed,[37] but differs drastically, revealing higher CNs (8 against 4−6 in $LiBH_4$[6] and 6 in $NaBH_4$[12]) and peculiar crystal chemistry. Clearly, the larger ionic radius for the metal cation favors higher CNs, and the higher pressure defines more and more dense arrangements of the BH_4 group inside its M-atom environment. Our conclusion that the stable configurations of the BH_4···M coordination define the crystal chemistry of metal borohydrides finds support in another example, $LiBH_4$. Even though the bonding between Li and BH_4 is mainly ionic, the directional Li···BH_4 interaction results in cation−anions layers, which determine the mechanisms of transitions between the polymorphic structures.[7,38] The stereochemical role of the anisotropic complex hydride anions has also been pointed out for the lithium amide-borohydride $Li_4BN_3H_{10}$.[33]

A note on more covalent metal borohydrides is warranted. The BH_4···M interaction involving less electropositive metals, such as Mg and Zn, appears more covalent, leading to even more directed and stable BH_4···M configurations. In such cases unexpected structural architectures appear, as doubly interpenetrated 3D frameworks in $MZn_2(BH_4)_5$[39] and a porous 3D framework in α-$Mg(BH_4)_2$.[34] These structural architectures are common for the coordination polymers involving organic ligands, such as MOFs, but they were only recently observed in metal hydrides. These observations highlight the structure-forming character of the directional BH_4···M interaction.

D. Raman Spectra. Selected Raman spectra recorded during a compression experiment from a $RbBH_4$ sample are shown in Figure 5. The evolution of the spectra shows three phase transitions, in agreement with X-ray diffraction data. The first phase transition is observed at around 2.5−2.7 GPa, the second phase transition at 7.5−8.2 GPa, and the third at about 19.7−21.3 GPa. The third transition (*C*222 → *I*-42*m* according to the XRD data) is somewhat less clear from Raman spectra due to an overall broadening of peaks and an unfortunate overlap for the region of bending modes of $RbBH_4$ with the broad peak from diamond anvils. The pressure dependence of the peak positions for the region up to 11 GPa is shown in Figure 6 and up to 24 GPa in Figure S5 of the Supporting Information.

Above 2000 cm^{-1}, there are strong Fermi resonances between the stretching modes (υ_1 and υ_3) with harmonics and combinations of the deformation modes ($2\upsilon_4$ and $\upsilon_2 + \upsilon_4$ and $2\upsilon_3$).[30,40] In particular, the bands observed at 2204 and 2240 cm^{-1} (at 1.4 GPa) are related to Fermi

(35) Gálvez Ruiz, J. C.; Nöth, H.; Warchhold, M. *Eur. J. Inorg. Chem.* **2007**, 251–266.
(36) Merrill, L. *J. Phys. Chem. Ref. Data* **1977**, *6*, 1205–1252.
(37) Vajeeston, P.; Ravindran, P.; Kjekshus, A.; Fjellvåg, H. *J. Alloys Compd.* **2005**, *387*, 97–104.
(38) Hagemann, H.; Filinchuk, Y.; Chernyshov, D.; van Beek, W. *Phase Trans.* **2009**, *82*, 344–355.
(39) Ravnsbæk, D.; Filinchuk, Y.; Cerenius, Y.; Jakobsen, H. J.; Besenbacher, F.; Skibsted, J.; Jensen, T. R. *Angew. Chem., Int. Ed.* **2009**, *48*, 6659–6663.
(40) Carbonnière, P.; Hagemann, H. *J. Phys. Chem. A* **2006**, *110*, 9927–9933.

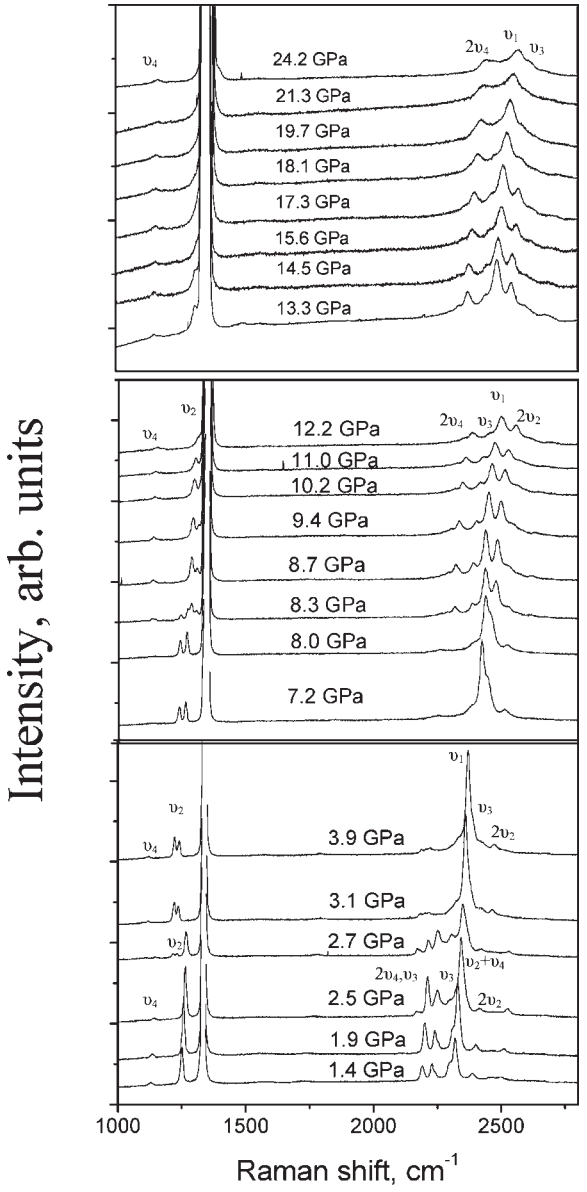

Figure 5. Raman spectra of $RbBH_4$ as a function of pressure at room temperature in the regions of phase transitions. The spectra were offset vertically for clarity. The strong peak, at ca. ~1330 cm^{-1}, is from the diamond anvils.

resonances of $2\upsilon_4$ with υ_1 and υ_3. At the first phase transition to the *P*4/*nmm* phase, the deformation modes υ_3 and υ_4 shift by about 30 cm^{-1} to lower frequencies, while the stretching modes do not follow this trend. This results in a reduced relative intensity of the two bands relative to $2\upsilon_4$, and the spectra are dominated by the totally symmetrical stretch υ_1. On the next phase transition (7.8 GPa), this behavior is reversed again and a complex stretching pattern is observed.

In the *P*4/*nmm* phase, the borohydride ion is located on a site with D_{2d} symmetry. The site group correlation table (Table 3) indicates that both bending modes υ_2 and υ_4 are expected to split into two components. Analysis of the symmetry of the zone center lattice vibrations (see Supporting Information) reveals no further splitting expected in the Raman spectra, as all the internal vibrations are split into g and u modes. The expected splitting is indeed observed experimentally: at 4.8 GPa, the υ_2 bands are

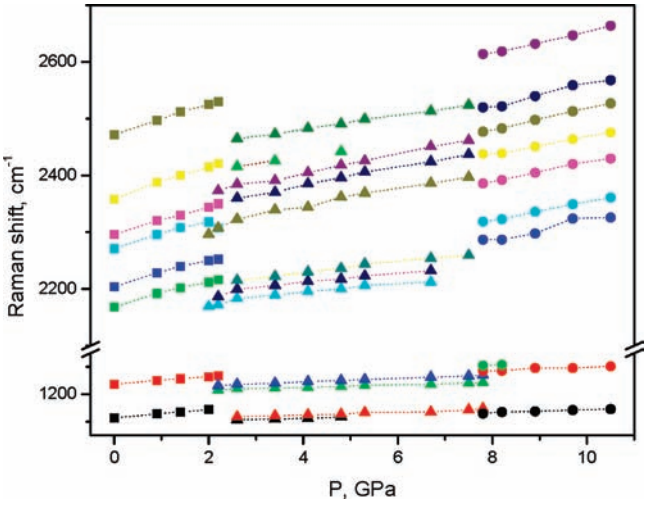

Figure 6. Pressure dependence of the Raman shift for $RbBH_4$ phases: squares represent the *Fm*-3*m*; triangles, *P*4/*nmm*; and circles, *C*222 phases.

Table 3. Site Group Correlation Table for the Internal Modes of the BH_4^- Ion

	T_d	D_{2d}	D_2
υ_1	A_1	A_1	A
υ_2	E	$A_1 + B_1$	2 A
υ_3	T_2	$B_2 + E$	$B_1 + B_2 + B_3$
υ_4	T_2	$B_2 + E$	$B_1 + B_2 + B_3$

observed at 1229 and 1250 cm^{-1}, and the weak υ_4 bands at 1117 and 1127 cm^{-1}. In the *C*222 phase (site symmetry D_2), the υ_3 and υ_4 modes are expected to split into three components. However, only two components of the υ_4 mode can be observed (at 1153 and 1183 cm^{-1} at 16.8 GPa). In the highest pressure phase (*I*-42*m*), the site symmetry is also D_2, and two bands are similarly observed for υ_4 at 1161 and 1213 cm^{-1} (at 23.7 GPa). The larger splitting suggests a stronger deformation of the BH_4^- ion from the parent T_d symmetry compared to the other polymorphs.

It has been shown that it is possible to relate the value of the totally symmetrical stretching mode (υ_1) of the BD_4^- ion to the B−D bond length using Badger's rule in the cubic alkali borodeuterides.[30] Recently, Racu et al. showed that Badger's rule is valid also for the orthorhombic $LiBD_4$.[41] This prompted us to apply this relation to the pressure-dependent data on $RbBD_4$. Experimentally, υ_1 shifts from 1593.7 at ambient pressure to 1606.6 cm^{-1} at 1.9 GPa. Using Badger's rule and the results of ref 30, one can estimate a reduction of the B−D bond length by ca. 0.015(5) Å. This result indicates that the relative compression of the BD_4^- ion (about 1.2%) is smaller than the compression of the unit cell (3.5%) seen from our diffraction data. A similar behavior was obtained theoretically using periodic DFT calculations under pressure for the RuH_6^{-4} ion in Ca_2RuH_6.[42]

Table 4 collects the observed mode Grüneisen parameters observed in the different phases. In the cubic *Fm*-3*m* phase, the Grüneisen parameter for all observed bands remains similarly weak (around 0.2), indicating

(41) Racu, A.-M.; Schoenes, J.; Łodziana, Z.; Borgschulte, A.; Züttel, A. *J. Phys. Chem. A* **2008**, *112*, 9716–9722.
(42) Daku, L. M. L.; Hagemann, H. *Phys. Rev. B* **2007**, *76*, 014118.

Table 4. Raman Shifts (cm^{-1}) and Mode Grüneisen Parameters $-d(\ln \nu)/d(\ln V)$ in the $RbBH_4$ Phases

Fm-3*m*	ν_4	ν_2	$2\nu_4,\nu_1$	$2\nu_4,\nu_3$	ν_3	ν_1	$\nu_2+\nu_4$	$2\nu_2$				
0 GPa	1113	1237	2168	2204	2271	2296	2358	2472				
	0.25	0.20	0.18	0.18	0.15	0.19	0.22	0.20				
*P*4/*nmm*	ν_4	ν_4	ν_2	ν_2	$2\nu_4$	$2\nu_4$	$2\nu_4$	ν_3	ν_1	ν_3	$2\nu_2$	$2\nu_2$
2.6 GPa	1107	1118	1220	1236	2183	2199	2215	2323	2360	2383	2416	2465
	0.16	0.21	0.17	0.24	0.18	0.19	0.19	0.32	0.30	0.31	0.20	0.22
*C*222	ν_4	ν_4	ν_2	$2\nu_4$	$2\nu_4$	ν_3	ν_1	ν_3	$2\nu_2$	$2\nu_2$		
12.8 GPa	1146	1173	1309	2335	2372	2441	2485	2539	2593	2672		
	0.09	0.28	0.19	0.24	0.27	0.23	0.25	0.26	0.26	0.30		
I-42*m*	ν_4	$2\nu_4$	ν_3	ν_1	ν_3							
20.8 GPa	1165	2430	2490	2548	2606							
	0.13	0.26	0.44	0.32	0.13							

thus a regular compression of the BH_4^- group. For RbBr, the mode Grüneisen parameters of the external translational modes were reported to be 1.67 and 2.42.[43] The significantly smaller values of the mode Grüneisen parameters for the internal BH_4^- modes shown in Table 4 confirm the observation reported above that the B−H bonds are much less compressed compared to the Rb···B distances. In the *P*4/*nmm* phase, however, a slight increase of the mode Grüneisen parameter is observed for the B−H stretching modes compared to the other bands (ca. 0.3 vs 0.2). At higher pressures, the observation of the deformation bands is restricted by the strong diamond Raman band at 1330 cm^{-1}. The difference in Grüneisen parameters for the two observed components of the υ_4 mode in the *C*222 phase reflects the increase of splitting with increasing pressure (increase of deformation). However, in the stretching mode region, the Grüneisen parameters of the combination bands and of the stretching modes are again similar (ca. 0.25), as in the cubic phase. The accuracy of the estimates of the Grüneisen parameters in the highest pressure phase is much lower due to the limited number of data points and the observed bandwidth (see Figure 5), so the values given in the table should be considered as indicative.

Conclusions

The pressure evolution of $RbBH_4$ has been characterized up to 23 GPa by synchrotron X-ray powder diffraction and Raman spectroscopy. Diffraction experiments at ambient temperature reveal three phase transitions: the ambient pressure *Fm*-3*m* polymorph transforms at 3.0 GPa into the new *P*4/*nmm* phase with a remarkable volume collapse of 8.8%, while the two transitions at higher pressures manifest a small volume drop of ~2.2% for the *P*4/*nmm* → *C*222 transition at 10.4 GPa and ~1.1% for the *C*222 → *I*-42*m* transition above 18 GPa.

The *P*4/*nmm* phase is an antitype to phosphonium iodide, while the *C*222 and *I*-42*m* phases represent two new structure types, which are the deformation variants of the cubic CsCl-type structure. The *P*4/*nmm* structure is an intermediate between NaCl and CsCl types, and all the transitions have the mechanism of atomic displacements. The BH_4 group acts with respect to Rb atoms as a mono-, di-, and trihapto ligand. It is the first time all three BH_4···M coordination modes are found in polymorphic modifications of the same compound. Different arrangements of the tetrahedral BH_4 group in the Rb environment result in different point group symmetries of the BH_4 anions as suggested by diffraction data and confirmed by Raman spectroscopy, i.e., $-4m2$ (D_{2d}) in the *P*4/*nmm* structure and 222 (D_2) in the *C*222 and *I*-42*m* structures, and define the crystal symmetries of the high-pressure $RbBH_4$ polymorphs. On the contrary, alkali metal halides, containing spherical cations and anions, show high symmetry cubic structures at various *P*−*T* conditions. In addition to structural data, we also present the individual Grüneisen parameters of the Raman-active phonon modes that may serve as a measure of the anharmonic vibrational response of the compression.

Our study shows that the structural chemistry of $RbBH_4$ under pressure is not identical to that of $NaBH_4$, as originally proposed, but differs drastically, revealing higher CNs and a peculiar crystal chemistry. The larger ionic radius for the metal cation favors higher CNs, and the higher pressure yields more and more dense arrangements of the BH_4 group inside its M-atom environment. The dense packing and realization of various BH_4···M coordination modes reflect a predominantly ionic character of $RbBH_4$. The less electropositive metals, such as Mg and Zn, form more complex structural architectures, such as an interpenetrated[39] and a porous[34] 3D framework.

Among all the borohydrides, $RbBH_4$ has the largest number of pressure-driven phase transitions. The only structure common to the whole MBH_4 family is the cubic one. Our analysis reveals a practically linear dependence of the compressibility of the cubic MBH_4 on the ionic radius of M. We conclude that its change in the series of cubic MBH_4 is largely defined by the compressibility of the repulsive BH_4···BH_4 interactions.

Acknowledgment. The authors acknowledge SNBL for in-house beam time allocation. This work was partly supported by the Swiss National Science Foundation. B.S. and A.T. acknowledge financial support from Carl Tryggers Stiftelse för Vetenskaplig Forskning and Magn. Bergvalls Stiftelse.

Supporting Information Available: Raman spectra of $RbBH_4$/$RbBD_4$/$RbBD_3H$; Rietveld refinement profiles and pressure dependence of the axial ratios for $RbBH_4$ phases; pressure dependence of Raman shifts and symmetry of zone center vibrations in $RbBH_4$ phases; crystal data as CIF files. This material is available free of charge via the Internet at http://pubs.acs.org.

(43) Hofmeister, A. M. *Phys. Rev. B* **1997**, *56*, 5835–5855.